Marquette University

e-Publications@Marquette

Electrical and Computer Engineering Faculty Research and Publications

Electrical and Computer Engineering, Department of

2-2011

Versatile Spectral Imaging With an Algorithm-Based Spectrometer Using Highly Tuneable Quantum Dot Infrared Photodetectors

Peter Vines

Chee Hing Tan

John P.R. David

Ram S. Attaluri

Thomas E. Vanderveldt

See next page for additional authors

Follow this and additional works at: https://epublications.marquette.edu/electric_fac

 Part of the Computer Engineering Commons, and the Electrical and Computer Engineering Commons

Authors

Peter Vines, Chee Hing Tan, John P.R. David, Ram S. Attaluri, Thomas E. Vanderveldt, Sanjay Krishna, Woo-Yong Jang, and Majeed M. Hayat

Marquette University

e-Publications@Marquette

Electrical and Computer Engineering Faculty Research and Publications/College of Engineering

This paper is NOT THE PUBLISHED VERSION; **but the author's final, peer-reviewed manuscript.** The published version may be accessed by following the link in the citation below.

IEEE Journal of Quantum Electronics, Vol. 47, No. 2 (February 2011): 190-197. DOI. This article is © Institute of Electrical and Electronic Engineers (IEEE) and permission has been granted for this version to appear in e-Publications@Marquette. Institute of Electrical and Electronic Engineers (IEEE) does not grant permission for this article to be further copied/distributed or hosted elsewhere without the express permission from Institute of Electrical and Electronic Engineers (IEEE).

Versatile Spectral Imaging With an Algorithm-Based Spectrometer Using Highly Tuneable Quantum Dot Infrared Photodetectors

Peter Vines
Department of Electronic and Electrical Engineering, University of Sheffield, Sheffield, U.K.
Chee Hing Tan
Department of Electronic and Electrical Engineering, University of Sheffield, Sheffield, U.K.
John P. R. David
Department of Electronic and Electrical Engineering, University of Sheffield, Sheffield, U.K.
Ram S. Attaluri
Lehigh University, Bethlehem, PA
Thomas E. Vandervelde
Tufts University, Medford, MA
Sanjay Krishna
Department of Electrical and Computer Engineering and Center for High Technology Materials, University of New Mexico, Albuquerque, NM
Woo-Yong Jang

Department of Electrical and Computer Engineering and Center for High Technology Materials, University of New Mexico, Albuquerque, NM

Majeed M. Hayat

Department of Electrical and Computer Engineering and Center for High Technology Materials, University of New Mexico, Albuquerque, NM

Abstract:

We report on the implementation of an algorithm-based spectrometer capable of reconstructing the spectral shape of materials in the mid-wave infrared (MWIR) and long-wave infrared (LWIR) wavelengths using only experimental photocurrent measurements from quantum dot infrared photodetectors (QDIPs). The theory and implementation of the algorithm will be described, followed by an investigation into this algorithmic spectrometer's performance. Compared to the QDIPs utilized in an earlier implementation, the ones used here have highly varying spectral shapes and four spectral peaks across the MWIR and LWIR wavelengths. It has been found that the spectrometer is capable of reconstructing broad spectral features of a range of bandpass infrared filters between wavelengths of 4 and 12 as well as identifying absorption features as narrow as 0.3 in the IR spectrum of a polyethylene sheet.

SECTION I. Introduction

Multispectral and hyperspectral imaging in the mid-wave infrared (MWIR) and long-wave infrared (LWIR) regions has attracted much interest due to a wide range of applications in areas such as advanced reconnaissance, chemical sensing, and atmospheric pollutant gas monitoring. Presently, multispectral imagers use optical filter wheels to filter radiation incident on a wideband IR detector [1]. The filters require cooling to prevent additional IR emission, which makes these systems operationally costly as well as bulky. Hyperspectral imagers use dispersive scanning optics to diffract the IR radiation and also use a wideband panchromatic detector [2], [3]. These moving parts make the system less reliable, bulkier, and costlier than purely electronic imagers. To achieve multicolor detection, a multijunction cadmium mercury telluride (CdHgTe) detector, with varying Cd compositions, has been adopted [4]. A similar approach to grow quantum well infrared photodetectors (QWIPs) with four spectral bands has also been demonstrated [5]. Achieving a high number of wavelength bands using this approach is difficult.

A novel flexible imaging technique has been proposed [6] as an alternative to these technologies. An algorithm combines the responses of a number of spectrally different detectors or a range of varied responses from a single detector using predetermined weighting factors to calculate the incident radiation as a function of wavelength across a specified wavelength range. Since this algorithmic spectrometer system can be preprogrammed with a specific spectral resolution and IR wavelength range, it can be highly flexible, and additionally, the absence of any optical filters or scanning optics makes the system potentially compact, cheap, and reliable. If the algorithmic spectrometer can operate with a single type of detector—one with a varying spectral response—the effective pixel area on 2-D multispectral focal plane arrays (FPA) can be increased without decreasing the spatial resolution of the FPA or altering the optical dimensions.

A number of detectors are in use in the MWIR and LWIR wavelength range. The well-established narrow-bandgap CdHgTe based detectors can detect a wide IR wavelength region [7], however, this range is usually fixed, meaning that a number of different structures would be required. QWIPs can be designed to exhibit a voltage-tunable spectral response [5]. However, the wavelength range covered is usually small and hence is not ideal for the system described above, although in principle different QW designs can be adopted to yield the desired spectral characteristics. By incorporating quantum dots in QWs, dot-in-a-well (DWELL) quantum dot

infrared photodetectors (QDIPs) can be designed to exhibit a spectral response that can be tuned across a wide wavelength range [8], [9], as well as providing normal-incidence detection. The spectral response of these detectors will vary as a function of the bias voltage applied across the detector, allowing one QDIP to effectively act as several separate detectors with differing spectral responses.

Sakoğlu et al. [6] have shown that the varying spectral response of DWELL QDIPs can be combined with the algorithmic spectrometer technique for multispectral or hyperspectral imaging. They reported that the spectrometer was able to reconstruct the smooth spectral shape of blackbody radiation using theoretically estimated photocurrents. The algorithm has since been extended to include a signal-to-noise ratio (SNR) term to increase the spectrometer's robustness to photocurrent measurement noise [10]. Recently, the algorithmic spectrometer has been used successfully to reconstruct the spectra of bandpass filters in the LWIR region from experimental photocurrent measurements [11].

Previous demonstrations of the algorithmic spectrometer have used QDIPs with spectral responses that have not been ideal for this purpose. In this paper, we will demonstrate the implementation of the spectrometer using more suitable QDIPs with highly variable spectral responses covering a broad IR wavelength range for imaging in both MWIR and LWIR regions. The technique will be demonstrated at 77 K, whereas previously most accurate reconstructions have been achieved at 30 K. We have been able to use this technique to capture narrow spectral features as well as the broad envelope of incident radiation over a wavelength range that is twice as great as previously achieved. Section II reviews the algorithmic spectrometer technique in more detail and Section IIIdetails the structure and characteristics of the QDIPs used. Section IV presents the results obtained using the algorithmic spectrometer.

SECTION II. Algorithmic Spectrometer Theory

The algorithmic spectrometer theory is described fully elsewhere [10], hence only an overview of the system will be provided here with the process detailed in Fig. 1. The spectrometer works on the principle that by summing the weighted spectral responses from any given number of bias voltages for a single QDIP, any desired arbitrary spectral shape can be approximated. For hyperspectral or multispectral imaging purposes, this spectral shape can take the form of a bandpass filter [with the triangular shape illustrated in Fig. 1(b), for example], thereby allowing a number of potentially wideband intrinsic responses from the detectors [as shown in Fig. 1(a)] to be combined to form an approximated narrowband response [as shown in Fig. 1(d) and (e)].

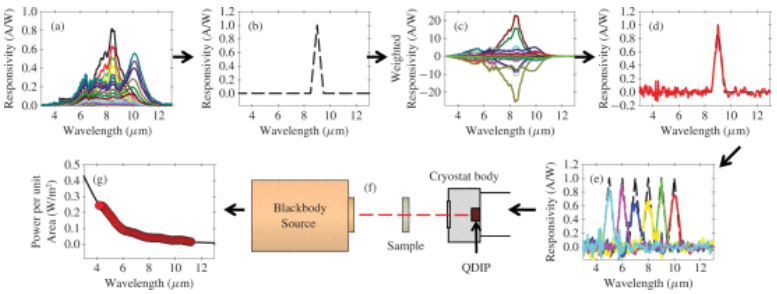

Fig. 1. Flow chart describing algorithmic spectrometer process. (a) Intrinsic QDIP responses at various applied bias voltages. (b) Desired arbitrary spectral shape—a narrow triangular bandpass filter. (c) Weighted intrinsic QDIP responses formed from multiplying the intrinsic QDIP responses by the associated weighting factors. (d) Sum of weighted intrinsic QDIP responses approximating the desired triangular bandpass filter. (e) Approximations of desired triangular bandpass filters with different center wavelengths. (f) Photocurrent measurement setup. (g) Final reconstruction of incident unfiltered blackbody radiation.

The algorithm approximates a desired spectral shape with an optimized least mean square error (MSE) fit by calculating a set of weighting factors with each weighting factor corresponding to the spectral response at a specific bias voltage

$$\boldsymbol{w} = (\boldsymbol{A}^T\boldsymbol{A} + \boldsymbol{\Phi})^{-1}\boldsymbol{A}^T R \quad (1)$$

where

$$\boldsymbol{A} = \begin{bmatrix} R_{V1}(\lambda_1) & R_{V2}(\lambda_1) & \cdots & R_{VM}(\lambda_1) \\ R_{V1}(\lambda_2) & R_{V2}(\lambda_2) & \cdots & R_{VM}(\lambda_2) \\ \vdots & \vdots & \vdots & \vdots \\ R_{V1}(\lambda_L) & R_{V2}(\lambda_L) & \cdots & R_{VM}(\lambda_L) \end{bmatrix} \quad (2)$$

and

$$\boldsymbol{R} = \begin{bmatrix} R(\lambda_1) \\ R(\lambda_2) \\ \vdots \\ R(\lambda_L) \end{bmatrix}. \quad (3)$$

The weighting factors are calculated using (1), where w is the weight vector corresponding to the set of weighting factors at each bias voltage (for measurements at M bias voltages a set of weights $w_1, w_2, \ldots, w_M$ will exist), $\boldsymbol{A}$ is the matrix formed by the intrinsic QDIP responsivities as a function of wavelength and applied bias voltage as shown in (2), and $\boldsymbol{R}$ is the desired arbitrary spectral shape as a function of wavelength shown in (3). The SNR term $\boldsymbol{\Phi}$ is described below, for ideal noiseless measurements it is a zero matrix.

In the reconstructions presented in this paper, $\boldsymbol{R}$ takes the form of a narrow triangular bandpass filter since it was found that the algorithmic spectrometer could produce better fits to this shape in an MSE sense when compared to the fits to the Gaussian or rectangular filter shapes which were assayed. The size of $\boldsymbol{A}$ is equal to $V \times \lambda$, where V is the number of bias voltages used by the spectrometer in the reconstruction and λ is the number of discreet responsivity readings in the wavelength range for both the intrinsic QDIP responsivities and the desired narrow triangular bandpass filters. The size of $\boldsymbol{A}$ varies from 4×1001 to 31×1001 in this paper.

Equation (1) can be calculated for any number of desired narrow triangular bandpass filters with different center wavelengths across the wavelength range of interest, each filter having its own specific set of weighting factors, thus providing the spectroscopy measurement capability.

Photocurrent measurements can then be made when the device is exposed to radiation from an object of interest. The incident power per unit area per unit wavelength at a specific wavelength λ_c can be approximated by taking a predetermined set of weights for the bandpass filter with center wavelength λ_c and summing the products of the photocurrent at each bias voltage and the corresponding weighting factor at that bias voltage. This is shown in (4), where $I_{V1}, \ldots, I_{VM}$ is the photocurrent at a specific bias voltage, $w_{Vi,\lambda c}$ is the weight for a specific bias voltage and center wavelength, and D_c relates the sum of the weighted photocurrents to the reconstructed incident power and is equal to the peak responsivity of the desired bandpass filter multiplied by the full-width-at-half-maximum (FWHM) of the desired bandpass filter

$$P_C = \frac{\sum_{i=1}^{M} w_{Vi,\lambda c} I_{Vi}}{D_c}. \quad (4)$$

The SNR term $\mathbf{\Phi}$ included in (1) can be incorporated into the algorithm to decrease the spectrometer's sensitivity to noise in the photocurrent measurements [10] arising from the equipment, background, and the detector. This has the effect of reducing the magnitude of the weighting factors and therefore reducing the accumulation of noise in the summation.

It is also possible to include a regularization term in the algorithm to avoid any spurious fluctuations in the resultant approximated spectra generally originating from the intrinsic QDIP spectra [10]. However, the QDIPs used here had strong intrinsic spectral responses which did not exhibit these fluctuations, and it was therefore found that including the regularization term did not yield a significant improvement to the bandpass filter approximations and the resultant spectral reconstructions.

SECTION III. QDIPs

The structure of the two QDIPs used by the spectrometer in this paper is shown in Fig. 2. Either 40 or 80 DWELL stacks were grown between two Si-doped $(2 \times 10^{18}\mathrm{cm}^{-3})\mathrm{n}^{+}$ GaAs regions. Each DWELL stack consisted of QDs grown using 2.0 monolayers of InAs with Si doping concentration of $1.4 \times 10^{11}\mathrm{cm}^{-2}$, giving approximately 1 electron/dot. The QDs are grown within a 20 Å$\mathrm{In_{0.15}Ga_{0.85}As}$ well (10 Å above the dot and 10 Å below), which in turn is situated in a 108.5 Å GaAs well (68.5 Å and 40 Å below). The DWELL regions were separated by 500 Å$\mathrm{Al_{0.1}Ga_{0.9}As}$ barriers. The wafers were fabricated using standard GaAs wet chemical processing techniques into circular mesa diodes with diameters of 200 and 400 μm and packaged using standard TO5 headers.

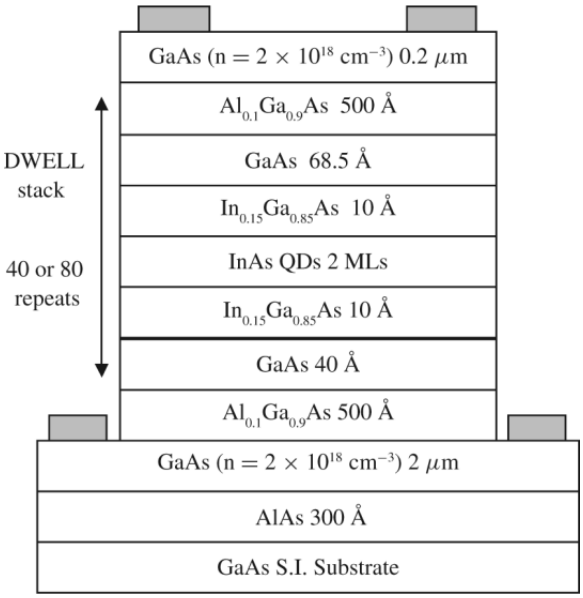

Fig. 2. Structure of the QDIPs used to evaluate the algorithmic spectrometer theory.

Dark current measurements were undertaken on both QDIPs at temperatures from 20 to 290 K as reported in other works [12], [13]. Fig. 3 shows that the dark current was constant between the two devices at a specific temperature and mean electric field (calculated by dividing the applied bias voltage by the intrinsic region width). Two important observations can be made from these results. First, no degradation in the dark current was observed with growth of up to 80 DWELL stacks indicating highly uniform growth of the QD layers and the

absence of strain accumulation in these devices. Second, the desired operating voltage can be obtained by selecting the appropriate number of DWELL stacks.

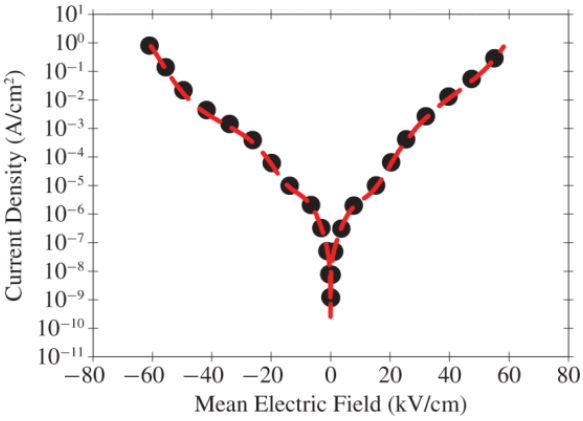

Fig. 3. Dark current at 77 K as a function of mean electric field for the 40-stack (black dotted line) and 80-stack (red dashed line) QDIPs.

Responsivity and noise current measurements at 77 K were used to calculate the detectivity D^* in these devices, as shown in Fig. 4. D^* is effectively constant between the two QDIPs for a given mean electric field confirming the highly uniform growth. The high D^* exhibited is important since it enables the algorithmic spectrometer to image with a narrow spectral resolution using larger weighting factors, allowing narrow spectral features to be reconstructed and imaging at a higher temperature than previously achieved.

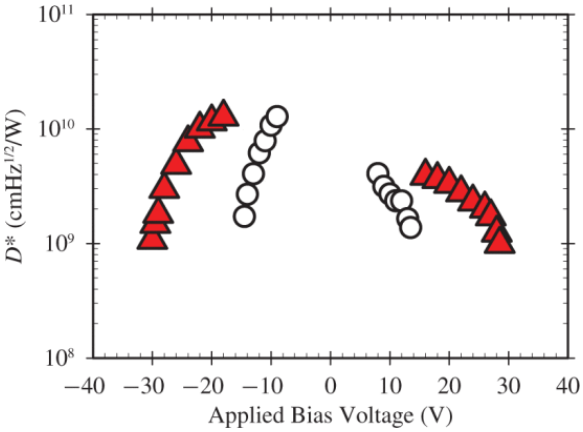

Fig. 4. D_* at 77 K as a function of mean electric field for the 40-stack (open circles) and 80-stack (red triangles) QDIPs.

The QDIP's spectral response was measured at 77 K using a Varian 7000 Fourier transform infrared spectrometer. It was found that the spectral response at any given mean electric field was identical between the two QDIPs confirming the uniform growth for the two structures.

Fig. 5 shows that the spectral response in the 80-stack QDIP varies significantly across the bias voltage range. The peak absorption wavelength was found to shift from 5.5 μmat −2V to 10 μm at +24V. It is this spectral diversity that makes these QDIPs ideally suited for use with the algorithmic spectrometer. Note that significantly higher applied bias voltages are possible in our QDIPs compared to those used in previous works [6], [10], [11] due to the thick intrinsic regions of 5.08 and 2.56 μm for the 80- and 40-stack QDIPs, respectively.

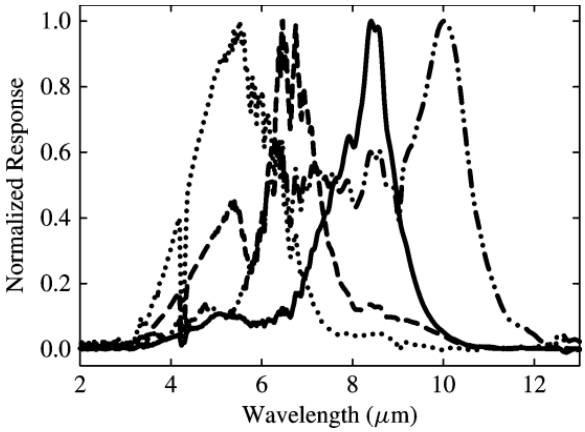

Fig. 5. Normalized spectral response at 77 K for the 80-stack QDIP at applied bias voltages of −18V(solid line), −2V (dotted line), +10V (dashed line), and +24V (dot-dashed line).

Fig. 6(a) shows that this spectral variation can be exploited by the algorithm to give excellent approximations to desired triangular bandpass filters with peak wavelengths ranging from 12.0 to 4.0 μm and an FWHM of 0.5 μm. A total of 31 different intrinsic spectral responses at bias voltages ranging from −29.5 to +28V were used in these approximations, with the resultant fits suitable to be used in reconstructing spectra with ideal noiseless photocurrent measurements. Note that the fitting is strongest between 5 and 10 μm—where the QDIP's responsivity is also strongest. Where the QDIP's responsivity is weaker—above 10 μm and below 5 μm—the approximations degrade in quality slightly but are still clearly identifiable. The noise floor in the reconstructed responsivities is due to the incomplete removal of responses outside the approximated filters' wavelengths. Fig. 6(b) shows that, if the number of spectra used in the approximation is reduced, then the MSE in the approximation increases although this is offset by a decrease in the time required to capture a single hyperspectral or multispectral image due to the reduced number of photocurrent measurements required. Therefore, it is important to optimize the algorithm to determine the smallest number of measurements required to yield a satisfactory reconstruction of the desired spectral shape, as discussed in more detail in Section IV.

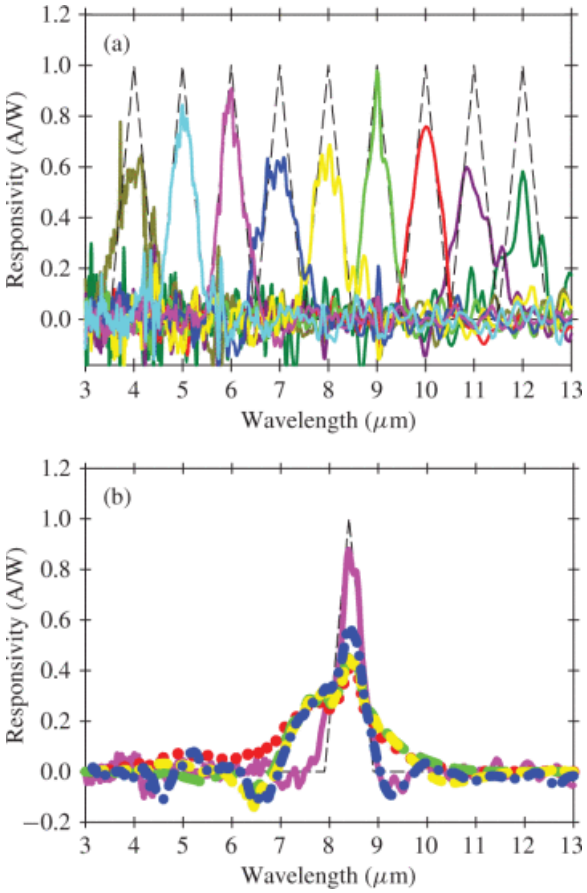

Fig. 6. (a) Triangular bandpass filter approximations (solid color lines) with FWHM of 0.5 μm formed from 31 QDIP spectra with center wavelengths ranging from 4.0 to 12.0 μm shown against the desired triangular bandpass filters (dashed black lines). (b) Fitting to a desired triangular bandpass filter with an FWHM of 0.5 μm and a center wavelength of 8.4 μm (dashed black line) using intrinsic QDIP spectra from 1 (red dotted line), 2 (green long dashed line), 4 (yellow short dashed line), 6 (blue dot-dashed line), and 31 (pink solid line) bias voltages.

SECTION IV. Algorithmic Spectrometer Evaluation

We will first examine the performance of the algorithmic spectrometer in the LWIR region. The algorithmic spectrometer was used to reconstruct an LWIR bandpass filter with cut-off wavelengths of 7.1 and 9.7 μm. The filter was placed between a blackbody source at a temperature of 800řC and the QDIP to form the spectrum shown in Fig. 7. Photocurrent measurements were taken using the QDIP with 80 DWELL stacks at 31 different bias voltages from −29.5 to +28V.

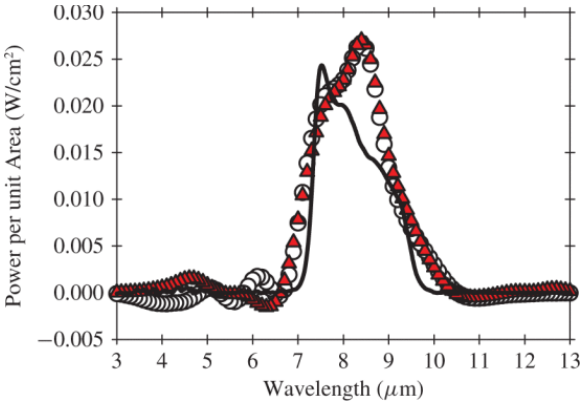

Fig. 7. LWIR filter spectrum (solid black line) reconstructed with 31 bias voltages (open circles) or 4 bias voltages (red triangles) and using triangular bandpass filters with FWHM of 0.5 μm.

It was found that the spectrometer could easily reconstruct the LWIR filter spectrum. Fig. 7 shows that the algorithmic spectrometer is able to reconstruct the filter characteristics using 31 bias voltages and triangular bandpass filters with an FWHM of 0.5 μm. Further analysis shows that excellent reconstructions can be achieved using as few as four bias voltages, allowing a very short radiation capture time. This is due to the strong intrinsic response of the QDIPs in the 7–10 μm range. The discrepancy around 8–9 μm is caused by errors in accurately approximating the triangular bandpass filters. Note that the MSE of these filters is higher than those depicted in Fig. 6(a) since in this case the algorithm has been made robust to photocurrent measurement noise. Although this SNR in the measured photocurrent is accounted for in the calculations of the weighting factors, this results in a higher error in the reconstruction of the target spectrum compared to an ideal reconstruction using theoretical noiseless photocurrent measurements due to the overestimation of the triangular filters in the 8–9 μm range. The discrepancy could be reduced by improving the SNR in the photocurrent measurements, thereby allowing more accurate bandpass filter approximations.

Selecting the optimum combination and number of bias voltages is dependent on the variation of the QDIP's spectral response across the wavelength range. When the number of bias voltages selected (out of the possible 31) is greater than 3, it is prohibitively time consuming to test the spectrometer with each combination due to the large number of combinations. For instance, if the spectrometer selects any 4 bias voltages out of a possible 31, then there are over 31 000 different combinations, and if any 6 biases are chosen, there are $\sim$730000 combinations. A detailed analysis of the optimal number and selection of bias voltages is outside the scope of this paper, however, our trials have shown that an accurate reconstruction across the wavelength range depends on two major factors. First, it is essential that the combined intrinsic QDIP responses are strong across the wavelength range to be reconstructed, if areas of the spectrum are only covered by weak responses, the reconstruction will also be weak in this area due to a poor approximation of the desired filters at this wavelength. Second, the intrinsic responses must vary in shape across the bias range to allow the algorithm many opportunities to fit to the desired filters. Therefore, the reconstructions achieved in this paper have used a set of bias voltages which have intrinsic QDIP spectra that cover the wavelength range of interest and have a roughly uniform variation in spectral shape from one bias voltage to the next.

Three further LWIR filters were used to demonstrate the versatility of the algorithmic spectrometer, as shown in Fig. 8. In these examples, 31 bias voltages from the QDIP with 80 stacks were used, with photocurrents calculated from the product of the QDIP's responsivity and the incident radiation. The three bandpass filters had cut-off wavelengths of 8.2–11.8, 8.5–10.2, and 10.0–11.5 μm. In reconstructing these spectra, the spectrometer has shown that it is capable of accurate reconstructions at wavelengths where the intrinsic response of the QDIP is relatively weak. The small oscillations away from the main peaks in the LWIR filter reconstructions are caused

by small errors in the desired filter approximations associated with these wavelengths. These errors occur at wavelengths where incident radiation is present, causing the algorithm to attribute this incident radiation to wavelengths were it is not present.

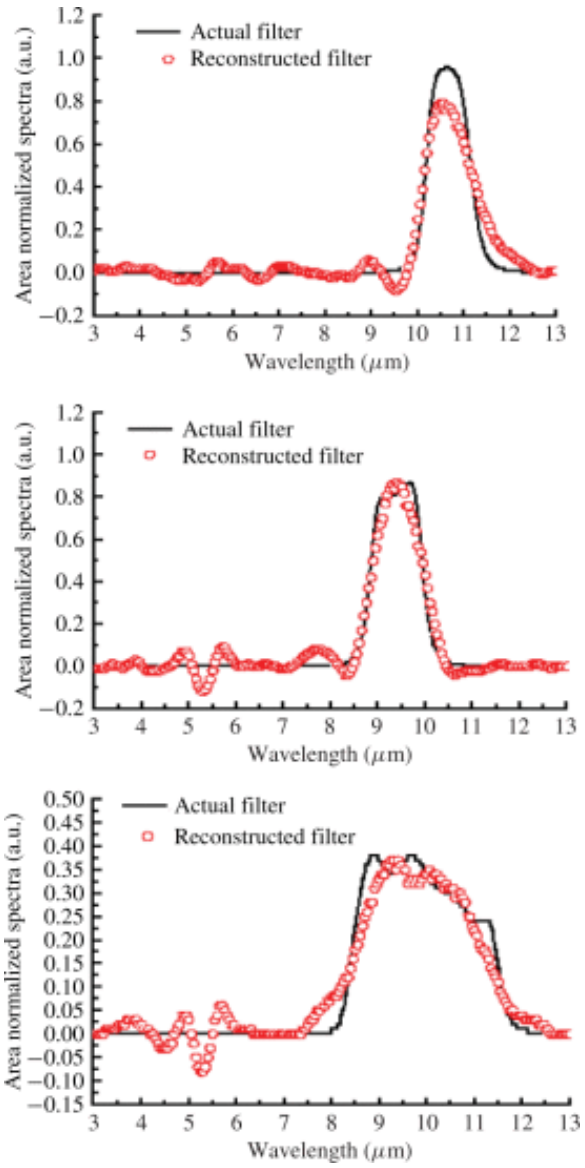

Fig. 8. Three LWIR bandpass filter spectra (solid black lines) reconstructed using 31 bias voltages and triangular bandpass filters with FWHM of 0.5 μm (red open circles).

The filters presented relatively simple spectra for the algorithmic spectrometer to reconstruct. A more stringent test using a polyethylene sheet was used to evaluate the spectrometer performance in the MWIR region. Polyethylene has a relatively strong transmission in the MWIR, where the intrinsic response of the QDIP is weak, and has a number of narrow spectral absorption features. It follows that a polyethylene sheet can be used to: 1) examine the algorithmic spectrometer performance in the MWIR, and 2) test the algorithmic spectrometer's capability in reconstructing narrow spectral features.

The photocurrent measurements were recorded with the polyethylene sheet placed between the QDIP and a blackbody source at a temperature of 800°C, and the resultant incident spectra are shown in Fig. 9. The 40 DWELL stack QDIP was used in order to reduce the operating voltage, and measurements were taken at 27 bias voltages from −14 to +13V.

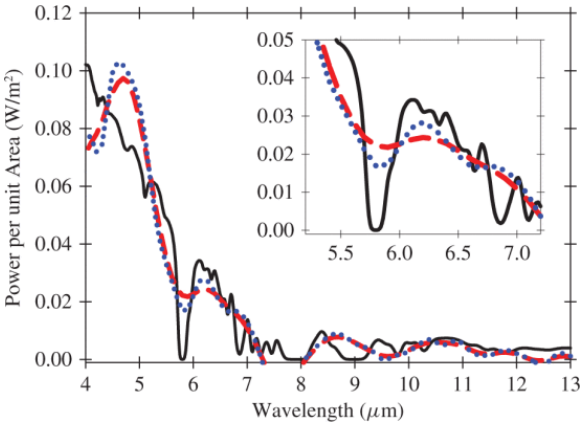

Fig. 9. Polyethylene sheet spectrum (black solid line) reconstructed with the algorithmic spectrometer using 27 bias voltages and a triangular band pass filter FWHM of 0.5 μm (red dashed line) or 0.25 μm (blue dotted line). Inset is enlarged around the absorption feature at 5.8 μm.

Results of using 27 bias voltages and triangular bandpass filters with an FWHM of 0.5 μm are shown in Fig. 9. The absorption features at 8 and 5.8 μm are clearly indicated, and the spectrometer gives a reasonably accurate reconstruction of the envelope of the power density.

Since the absorption feature at 5.8 μm has a narrower width (0.3μm) than the triangular bandpass filter's FWHM (0.5μm), it is challenging to capture it correctly. If the FWHM of the triangular bandpass filters is reduced, it is possible to improve the reconstruction of narrow features. Fig. 9 also shows the polyethylene reconstruction using triangular bandpass filters with an FWHM of 0.25 μm. The 5.8 μm feature is now more pronounced in the reconstruction. Reducing the FWHM of the bandpass filters below 0.25 μm does not produce any further improvements in the reconstruction due to the poor approximation to very narrow bandpass filters. This is due to the need for larger weighting factors for approximations with very narrow FWHM, which leads to an increase in the cumulative effect of measurement noise.

An attempt to minimize the number of bias voltages required to reconstruct the polyethylene spectrum was carried out. When the number of bias voltages is reduced to 14, the measurement time required to reconstruct the spectrum was approximately halved, and Fig. 10 shows that the quality of the reconstruction does not degrade. Since the 14 bias voltages can still cover the QDIP's intrinsic spectral shapes and peaks, the narrowband filter approximations do not alter significantly, allowing the polyethylene spectrum to be reconstructed with a similar accuracy as with 27 biases. Reducing the number of bias voltages further gradually causes some of the QDIP's intrinsic spectral shapes to be lost and the resultant reconstruction degrades accordingly. However, our results show that the algorithm-based spectrometer is a promising approach toward achieving a highly adaptable IR sensor.

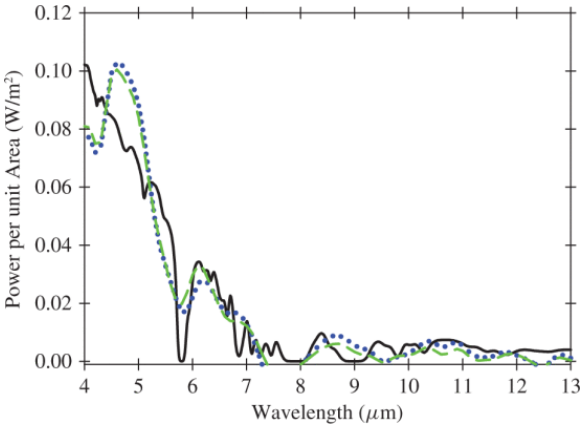

Fig. 10. Polyethylene sheet spectrum (black solid line) reconstructed with the algorithmic spectrometer using triangular bandpass filters with FWHM of 0.25 μm and using 27 bias voltages (blue dotted line) or 14 bias voltages (green dashed line).

Further improvements to the reconstruction are possible if the SNR can be increased. This will allow the narrow bandpass filters to be better approximated since, as the spectrometer does not need to be as robust to measurement noise, larger weighting factors may be used [10]. Decreasing the QDIP's operating temperature reduces the dark current and noise current and is therefore one way to achieve further improvement in the spectral reconstruction.

SECTION V. Conclusion

The algorithmic spectrometer reported in [10] has been demonstrated at higher temperatures than previously reported using QDIPs with spectral responses that vary significantly with applied bias voltage. Spectrometer testing showed that it was capable of reconstructing broad features in the 4–12 μm region using few bias voltages, thus allowing for a short radiation capture time. At present, determining the minimum number of bias voltage to use as well as the combination of these measurements is not trivial. This paper suggested that selecting the spectral responses which differ significantly in spectral shape and together cover a large wavelength range will provide the best set of data to be used during the reconstruction. It has been possible to capture spectral features as narrow as 0.3 μm using the desired triangular bandpass filters with an FWHM of a similar magnitude. Although the QDIPs used at present have operating voltages that are too high for FPA integration, they would be ideal for single-pixel applications. Furthermore, it should be possible to reduce the intrinsic width of the QDIPs to give an FPA suitable detector. Extensive testing and evaluation will ensure that an application-specific optimal system can reconstruct unknown targets within the shortest possible capture time over the specified wavelength range required and with the specified spectral resolution, and will allow the spectrometer reconstruction accuracy to be quantified. While we have achieved encouraging results using a fairly simple algorithm, further developments including improvements the QDIP designs with wider spectral tunability and improvements to the algorithm could lead to a new class of multi/hyperspectral imaging-on-the-chip capability.

References

1. L. G. Hipwood, I. M. Baker, C. L. Jones, C. Maxey, H. W. Lau, J. Fitzmaurice, M. Wilson, P. Knowles, "LW IRFPAs made from HgCdTe grown by MOVPE for use in multispectral imaging", *Proc. SPIE Infrared Technol. Appl.*, vol. 6940, pp. 69400G-69400G, 2008-Apr.

2. N. Gupta, D. Smith, "A field-portable simultaneous dual-band infrared hyperspectral imager", *Proc. AIPR*, pp. 87-93, 2005.

3. M. Hinnrichs, N. Gupta, "Comparison of QWIP to HgCdTe detectors for gas imaging", *Proc. SPIE Infrared Technol. Appl.*, vol. 6940, pp. 69401Q-1-69401Q-9, 2008.

4. L. G. Hipwood, C. L. Jones, C. D. Maxey, H. W. Lau, J. Fitzmaurice, R. A. Catchpole, M. Ordish, "Three-color MOVPE MCT diodes", *Proc. SPIE Infrared Technol. Appl.*, vol. 6206, pp. 620612-620612, 2006.

5. S. D. Gunapala, S. V. Bandara, J. K. Liu, S. B. Rafol, J. M. Mumolo, " 640 \$times\$ 512 pixel long-wavelength infrared narrowband multiband and broadband QWIP focal plane arrays ", *IEEE Trans. Electron Devices*, vol. 50, pp. 2353-2360, Dec. 2003.

6. . Sakolu, J. S. Tyo, M. M. Hayat, S. Raghavan, S. Krishna, "Spectrally adaptive infrared photodetectors with bias-tunable quantum dots", *J. Opt. Soc. Am. B*, vol. 21, no. 1, pp. 7-17, Jan. 2004.

7. J. Beck, C. Wan, M. Kinch, J. Robinson, P. Mitra, R. Scritchfield, F. Ma, J. Campbell, "The HgCdTe electron avalanche photodiode", *J. Electron. Mater.*, vol. 35, no. 6, pp. 1166-1173, Jun. 2006.

8. S. Raghavan, P. Rotella, A. Stintz, B. Fuchs, S. Krishna, C. Morath, D. A. Cardimona, S. W. Kennerly, " High-responsivity normal-incidence long-wave infrared \$(lambdasim 7.2~mu{rm m})~{rm InAs}/{rm In}_{0.15}{rm Ga}_{0.85}{rm As}\$ dots-in-a-well detector ", *Appl. Phys. Lett.*, vol. 81, no. 8, pp. 1369-1371, Aug. 2002.

9. S. Krishna, S. Raghavan, G. von Winckel, A. Stintz, G. Ariyawansa, S. G. Matsik, A. G. U. Perera, " Three-color \$lambda_{{p}^{1}}sim 3.8~mu{rm m}\$ \$lambda_{{p}^{2}}sim 8.5~mu{rm m}\$ \$lambda_{{p}^{3}}sim 23.2~mu{rm m}\$ InAs/InGaAs quantum-dots-in-a-well detector ", *Appl. Phys. Lett.*, vol. 83, no. 14, pp. 2745-2747, Oct. 2003.

10. Sakolu, M. M. Hayat, J. S. Tyo, P. Dowd, S. Annamalai, K. T. Posani, S. Krishna, "Statistical adaptive sensing by detectors with spectrally overlapping bands", *Appl. Opt.*, vol. 45, no. 28, pp. 7224-7234, Oct. 2006.

11. W.-Y. Jang, M. M. Hayat, J. S. Tyo, R. S. Attaluri, T. E. Vandervelde, Y. D. Sharma, R. Shenoi, A. Stintz, E. R. Cantwell, S. C. Bender, S. J. Lee, S. K. Noh, S. Krishna, "Demonstration of bias-controlled algorithmic tuning of quantum dots in a well (DWELL) midIR detectors", *IEEE J. Quantum Electron.*, vol. 45, pp. 674-683, Jun. 2009.

12. P. Vines, C. H. Tan, J. P. R. David, R. S. Attaluri, T. E. Vandervelde, S. Krishna, "Noise gain and responsivity in low strain quantum dot infrared photodetectors with up to 80 dot-in-a-well periods", *IEEE J. Quantum Electron.*.

13. P. Vines, C. H. Tan, J. P. R. David, R. S. Attaluri, T. E. Vandervelde, S. Krishna, "Multiple stack quantum dot infrared photodetectors", *Proc. SPIE Electro-Opt. Infrared Syst.: Technol. Appl.*, vol. 7113, pp. 71130J-71130J, 2008.